Dalton
Transactions

RSC**Publishing**

An interpenetrated bioactive nonlinear optical MOF containing coordinated quinolone-like drug and Zn(II) for pH-responsive release

Li-Na Duan, Qin-Qin Dang, Cai-Yun Han, Xian-Ming Zhang[*]

A new interpenetrated bioactive nonlinear optical metal-organic framework [$Zn_2(ppa)_2(1,3\text{-}bdc)(H_2O)$] has been designed and synthesized, which shows both a high drug content of 63.9% and a good slow release effect in simulated physical conditions compared to other noninterpenetrated bioactive MOFs. It also shows large powder second-harmonic generation (SHG) efficiency of 5.6 times of KH_2PO_4 (particle size: 150−200 μm).

Introduction

Metal–organic frameworks (MOFs) have captivated great attention of chemists due to their tremendous potential applications in gas storage, ion exchange, microelectronics, nonlinear optics, and catalysis.[1] Besides, MOFs can be regarded as good candidates for drug delivery systems owing to their high drug loadings, biodegradability and versatile functionality.[2] Since Ferey and colleagues first reported MOFs could encapsulate drug molecules within the pores and release slowly in 2006,[3] some advances have been made in MOFs as drug delivery systems. Lin et al. have prepared a Pt-based drug that has been used for creating coordination framework.[4] Horcajada and co-workers encapsulated ibuprofen within the flexible microporous metal terephthalate MIL-53s.[5] An et al. reported an important encapsulation and delivery of cationic drug (procainamide) from an anionic pillared zinc-adeninate MOF in phosphate buffer solution (PBS).[6] In 2010, Horcajada, Gref and co-workers have shown that porous nanoparticles of iron carboxylate MOFs can adsorb and release several highly challenging drugs, such as the antitumoral busulfan (Bu) or doxorubicin (Doxo) and the antiviral azidothimidine triphosphate (AZT-Tp) or cidofovir (CDV).[7] Until now, most of drug delivery from MOFs has been achieved by impregnation of MOFs in a saturated solution of drug, which strongly depends on the porosity and volume and results in uncertain encapsulation. On the other hand, MOFs are likely to degrade in the body, inevitably raising additional toxic concerns. Serre and co-workers developed another drug delivery approach to construct "bioactive MOF" through direct coordination of biomolecule vitamin B3 with non toxic metal Fe ions.[8] However, the resulting material degrades rapidly under physiological conditions. Spencer demonstrated that deferiprone treatment for haemosiderosis can be included as a ligand in "bioactive MOFs" based on zinc.[9] Similarly, deferiprone is immediately released from the MOFs upon treatment with PBS buffer. The burst release of drug molecules from the two "bioactive MOFs" may be related to their loose and non-interpenetrated structures. In addition, second-order

nonlinear optical (NLO) materials have attracted considerable research interest due to their important applications in optoelectronic technologies.[10] The second-harmonic generation (SHG) properties originate from the charge transfer as a result of the strong push-pull effect in the donor-acceptor type of molecules. Longer bridging ligands has better conjugation between the donor and the acceptor which can enhance the molecular hyperpolarizability (β) of NLO. Herein, we are developing another approach to build up "bioactive MOFs" with controlled release property, namely, interpenetrated structure with drug molecule directly coordinated to Zn(II). The interpenetration may enhance stability of this bioactive MOF and avoid fast release of drug molecules. This "bioactive MOFs" crystallize in noncentrosymmetric space groups and has been found to be SHG active.
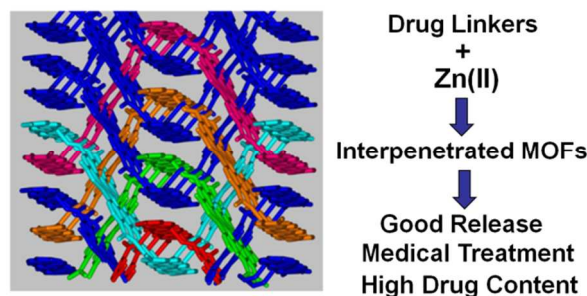
Considering the above points, therapeutic molecule pipemidic acid (Hppa) and low toxic 1,3-benzenedicarboxylate as ligands and Zn(II) were used to build up "bioactive MOFs". Hppa is active against many pathogenic bacterial species (both Gram-negative and Gram-positive) as gyrase inhibitors and has a very broad clinical application in the treatment and prevention of respiratory, enteric, and urinary tract infections.[11] Hppa with large π-conjugated system can produce compounds with excellent SHG properties. Zinc is an essential nutrient element for life in the dose range which can be used as an antibacterial growth agent.[12] In nonlinear optically active MOFs, Zn^{2+} is

Dalton Transactions Accepted Manuscript

commonly used as connecting points to avoid unwanted *d-d* transitions in the visible region. It is expected that integration of Hppa and Zn(II) as well as dicarboxylate ligand could lead to interpenetrated MOFs, which not only can achieve the purpose of medical treatment but also show low toxicity values. In this work, we report a bioactive MOF, namely [Zn$_2$(ppa)$_2$(1,3-bdc)(H$_2$O)]·2H$_2$O (**1**), which shows both a high drug content and a good slow release effect in simulated physical conditions compared to other noninterpenetrated bioactive MOFs. In addition, **1** with a large SHG demonstrated its potential for application in the field of nonlinear optical materials.

EXPERIMENTAL SECTION

Materials and Methods

UV-vis absorption was monitored with a Varian Cary 100 Scan spectrophotometer. Scanning electron micrographs (SEM) were recorded in a JSM-7500F. X-ray powder diffraction (XRPD) data were recorded in a Bruker D8 ADVANCE X-ray powder diffractometer (Cu$_{K\alpha}$, λ = 1.5418 Å). Photoluminescence analysis was performed on an Edinburgh FLS920 luminescence spectrometer. The FT-IR spectra were recorded from KBr pellets in range 400-4000 cm^{-1} on a Perkin-Elmer Spectrum BX FT-IR spectrometer. Elemental analysis was performed on a Vario EL-II elemental analyzer.

Syntheses

A mixture of Zn(OAC)$_2$·2H$_2$O (0.044g, 0.2 mmol), Hppa (0.071g, 0.2 mmol), 1,3-H$_2$bdc (0.033g, 0.2mmol), NaOH (0.021g, 0.5mmol) in H$_2$O (8 mL) was sealed in a 25 mL Teflon-lined stainless steel container, which was heated at 130 ^{o}C for 3 d and then cooled down to room temperature at a rate of 5 ^{o}C h^{-1}. Yellow crystals of **1** were collected and washed with distilled water and dried in air to give the product; yield, 68% based on Zn. Anal. Calc. for C$_{36}$H$_{38}$Zn$_2$N$_{10}$O$_{13}$ (**1**): C, 45.54; H, 4.03; N, 14.75. Found: C, 45.29; H, 4.52; N, 15.47%.

Degradation tests

According to the molar ratio of the compound **1**, a mixture solution of 0.4 mM of Zn(OAc)$_2$·H$_2$O, 0.4 mM of Hppa and 0.2 mM of 1,3-H$_2$bdc was prepared as standards and the pH was controlled by HCl (PH 2.0) before being diluted to volume. This change in UV absorbance was normalized for clarity in comparison. The final solution was spectrophotometrically analyzed in the UV-vis region after reaching a stable state. UV-absorbance of standard solutions was measured at wavelengths of 275 nm as well in compound **1** release as pipemidic acid. The absorption maximum of 1,3-benzenedicarboxylate was at 211 nm (Fig. S2 and S3, ESI†).

In a typical release experiment, compound **1** (10mg) in a dialysis bag (cut-off molecular weight: 3500) was released under simulated physiological conditions of different pH (37°C, bidimensional stirring at 100 rpm). The release medium were simulated gastric fluid (SGF, 0.01M HCl solution pH 2.0), simulated body fluid (SBF, NaH$_2$PO$_4$–Na$_2$HPO$_4$ buffer solution pH 7.4) and simulated intesrinum crassum fluid (SIC, NaHCO$_3$ buffer solution pH 8.3). The dispersion was dialyzed against 200ml of solution for 48h. At each time point, 1ml solution were removed and replaced with fresh solution. Experiment was done in triplicate. The aliquot was then analyzed by UV-vis spectroscopy. Crystals of **1** was ground and sieved into a

series of distinct particle size ranges of 25−40 μm and 63−80 μm. The tablets of **1** were prepared under 15MPa.

Crystallographic studies

X-ray single-crystal diffraction data for **1** was collected on a Bruker Smart APEX CCD diffractometer at 298(2) K using Mo Kα radiation (λ = 0.71073 Å). The program SAINT was used for integration of the diffraction profiles, and the program SADABS was used for absorption correction. The structure was solved by direct method using the SHELXS program of the SHELXTL package and refined by full-matrix least-squares technique with SHELXL. All nonhydrogen atoms were refined with anisotropic thermal parameters. Hydrogen atoms of organic ligand were generated theoretically onto the specific carbon and refined isotropically with fixed thermal factors. Hydrogen atoms of the water molecules could not be determined and are not included in the model. Further details for structural analysis are summarized in Table S1, ESI† and selected bond lengths and angles are shown in Table S2, ESI†.

Second Harmonic Generation Measurements

The measurements of the powder frequency-doubling effects for **1** were carried out on the sieved samples by means of the modified method of Kurtz and Perry. Crystals of **1** were ground and sieved into a series of distinct particle size ranges of 25−40, 40−63, 63−80, 80−125, and 125−150 μm, respectively, which were pressed into a disk with diameter of 8 mm that was put between glass microscope slides and secured with tape in a 1-mm thick aluminum holder, and powdered KH$_2$PO$_4$ sample used as the reference was sieved into the same size range.

RESULTS AND DISCUSSION

Description of Structures

Compound **1** features 2D acentric structure constructed from undulating 2D honeycomb networks via parallel 3-fold interpenetration of (6,3) networks, in which the therapeutically active pipemidic acid are directly coordinated to essential Zn(II). It crystallizes in monoclinic acentric space group Cc and the asymmetric unit contains two Zn(II), two ppa ligands, one 1,3-bdc and three water molecules (Fig. 1a). The Zn1 center exhibits a distorted trigonal-bipyramidal coordination environment (Scheme S1. ESI†), defined by two carboxylate oxygen atoms from 1,3-bdc, two oxygen atoms and one nitrogen from ppa groups. The Zn2 center adopts a distorted octahedral geometry, coordinated by two carboxylate oxygen atoms from 1,3-bdc, two oxygen and one nitrogen atom from ppa ligands, and one water. The 1,3-bdc ligand adopts a chelating bis(bidentate) coordination mode while ppa ligand acts as a tridentate bridged ligand to link two Zn(II). Based on these connections, Zn(II) are bridged by ppa and 1,3-bdc ligands alternately to generate a 2D open (6,3) layer with very large hexagonal rings (Fig. 1b). The size of the window is estimated from the distance between two Zn(II) to be 21.6 Å × 24.1Å. The layer is highly undulating and the voids of a single layer are so large that allow other two undulating layers to penetrate in a parallel manner, giving 2D-2D 3-fold interpenetrating (6,3) network (Fig. 1c). According to the calculation of PLATON, **1** is nonporous. The network of **1** is 2D-2D 3-fold interpenetrating (6,3) nets (Fig. S1, ESI†).

(a)

(b)

(c)
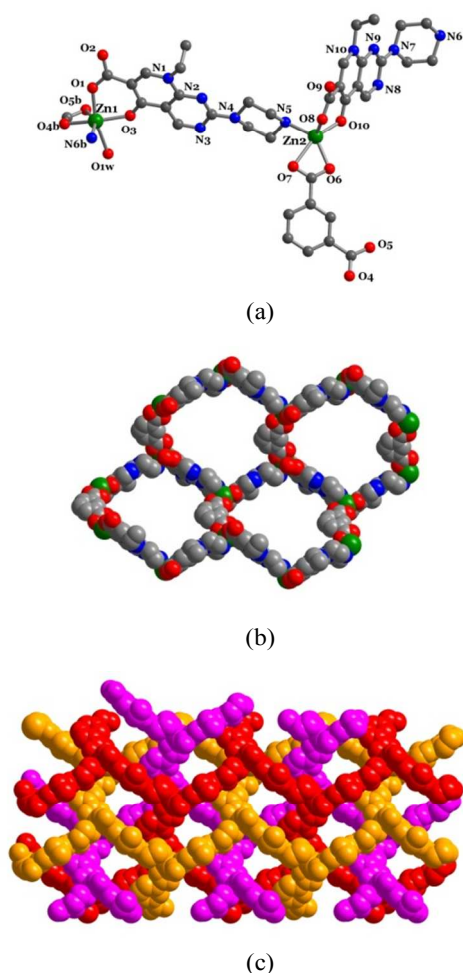
Fig. 1 Coordination environments of Zn(II) (a), space filling view of a single (b) and three-fold interpenetrated 2D networks in **1**(c). Symmetry code in (a): b) 1/2+x,1/2+z,3/2+z.

Thermal Stability Studies

TGA curves of **1** in nitrogen at the rate of 10 °C/min. There are three steps of weight losses (Fig. S7, ESI†). The first weight loss is 5.23% in the temperature range of 45-135 °C, which corresponds to the loss of non-coordinated and coordinated water molecules. Then the sample keeps relatively stable in the temperature range of 135-330 °C. The second weight loss is 43.37% at 330-495 °C and the last step is 33.36% in the temperature range of 495-680 °C, indicating the complete deposition of the complex to form ZnO as a final product. This conclusion is supported by the percentage of the residues, which is in accordance with the calculated value (17.15%).

Degradation of 1 with different particle size under different pH conditions

Compound **1** contains drug content as high as 63.9%, and in vitro release experiments have been investigated in SGF, pH 2.0, SBF, pH 7.4 and SIC, pH 8.3 respectively. Besides, the release rate of drugs may be associated with the particle size of **1**, so we tested the degradation of **1** with different particle size including 25−40 μ m, 63−80 μ m and pressed tablets, which

were characterized by SEM (Fig. S4, ESI†). The release profile of Hppa was presented in Figure 2 (particle size ranges 25−40 μ m). A progressive release was observed with no "burst effect" under SGF, SBF and SIC respectively. Within 48 hours, approximately 100% of Hppa was released in SGF and **1** had a half life ($t_{1/2}$) of ~1.5 h. However, only 90.1% and 38.1% of drug was degradated in a comparative experiment in SBF and SIC, respectively. **1** gave a $t_{1/2}$ of ~7 h and ~18 h in SBF and SIC. The release profile of **1** with 63−80 μm and pressed tablets was presented Figure S5 and Figure S6. The half life of different particle sizes in SGF, SBF and SIC were summarized in table S1. According to the table S1, the smaller the particle size is, the faster degradation is. The possible reason may attribute to specific surface area. In addition, regardless of the particle size of **1**, the release rate of Hppa is the fastest in SGF compare with SBF and SIC. Compared with other bioactive MOF such as BioMIL-1[8] and deferiprone based MOFs[9] with a full release in two hours in PBS, the degradation of **1** is significantly retarded, presumably due to the interpenetrated structure of **1**.
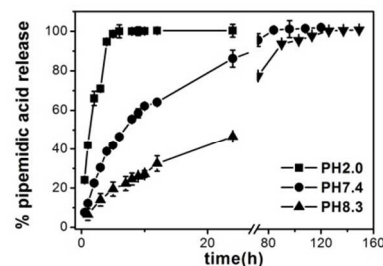
Fig. 2 pH-responsive release of pipemidic acid from compound **1** (particle size ranges 25−40 μm) under simulated physiological conditions.

The release amount of Hppa increases with decrease of pH value. The possible reason is that both Zn(II) and protons are Lewis acids and compete to combine with ppa group. In solution of SGF (pH 2.0), protons have more opportunities to combine with ppa group compared with in SBF and SIC, which leads to a full degradation of **1** and a large release rate.[13] Compound **1** dissolved in SGF after a full degradation. While white insoluble solids formed after degradation in SBF and SIC which may be insoluble zinc phosphates and zinc carbonate respectively, according to the chemistry of zinc (Pourbaix diagram).[14] The insoluble solids is further characterized by XRPD (Fig. 3) and IR spectroscopy (Figure S8). Interestingly, in the case of compound **1**, the degradation products, zinc and 1,3-bdc, are endogenous, and show low toxicity values (LD_{50}(Zn) = 0.35 g kg^{-1}, LD_{50}(1,3-bdc) = 10.4 g kg^{-1}).[15] Their non-toxic nature and unusually large contents of drug make them ideal candidates in the field of delivery of the bioactive molecule.

Dalton Transactions Accepted Manuscript
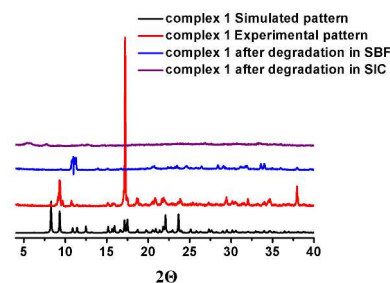
Fig. 3 XRPD patterns of **1** and the simulated XRPD from the single-crystal X-ray structure

SHG Properties

Second-Harmonic Generation (SHG) measurements of powdered **1** were performed on a modified Kurtz-NLO system using a pulsed Nd:YAG laser with a wavelength of 1064 nm.[16] As powder SHG efficiency has been shown to depend strongly on particle size, materials were ground and sieved into distinct particle size ranges (25−40, 40−63, 63−80, 80−125, 125−150 μm) as illustrated in Figure 4. The **1** exhibits high transparency (above 80%) in the range of 350−800 nm (Fig. S8, ESI†). The SHG intensity for **1** is about 5.6 times that of technologically important potassium dihydrogen phosphate (KDP) in the particle size of 150−200 μm. Particle size vs SHG efficiency data indicate that **1** is type I phase-matchable. The large SHG efficiency may be attributed to the longer bridging Hppa ligands which exhibit better conjugation between piperazine-N donor and the carboxylate-acceptor, which is known to enhance the molecular hyperpolarizability of inorganic second-order nonlinear optical (NLO) Chromophores.
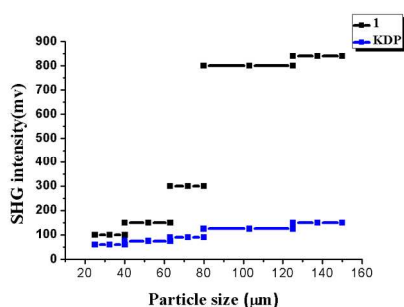
Fig. 4 Particle size vs SHG intensity for **1** showing type I phase-matching curve.

Photoluminescent properties

Due to the excellent luminescent properties of d^{10} metal complexes, the solid-state luminescence of the three compounds was investigated at room temperature.[17] It can be observed that intense emissions occur at 442 nm (Fig. 4, λ_{ex}= 345 nm) for **1**. For free Hppa it was found that one weak emission at 506 nm could be observed. Therefore, the emission of **1** may be attributable to ligand-to-metal charge transfer (LMCT). The enhancement of fluorescent emission intensity may be attributed to coordination of Hppa to metal ions increasing the ligand conformation rigidity, which reduces the nonradioactive decay of the intraligand excited state.
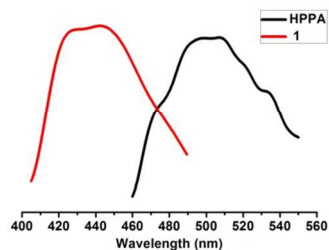
Fig. 4 Photoluminescent spectra of **1** and free Hppa ligand in solid state at room temperature upon excitation 345 nm.

Conclusions

In summary, we develop another approach to "bioactive MOFs" with controlled degradation properties, namely, interpenetrated structure with drug pipemidate directly coordinated to Zn(II). This bioactive MOF combined high drug content of 63.9% and good release effect, which is suitable to be used as drug delivery system. The interpenetration enhanced stability of this bioactive MOF and avoided fast release of drug molecules. In addition, this acentric bioactive MOF shows large SHG efficiency of 5.6 times of technologically important KDP.

Acknowledgements

References

1   (a) J. Lee; O. K. Farha, J. Roberts; K. A. Scheidt, S. T. Nguyen and J. T. Hupp, *Chem. Soc. Rev.* **2009**, *38*, 1450(b) C. Wang; T. Zhang and W. Lin, *Chem. Rev.* **2012**, *112*, 1084(c) S. Horiuchi, F. Kagawa, K. Hatahara, K. Kobayashi; R. Kumai, Y. Murakami and Y. Tokura, *Nat. Commun.* **2012**, *3*, 1308(d) S. Yang, S. K. Callear, A. J. Ramirez-Cuesta, W. I. F. David, J. Sun, A. J. Blake, N. R. Champness and M. Schroder, *Faraday Discuss.* **2011**, *151*, 19(e) D. J. Tranchemontagne, K. S. Park, H. Furukawa, J. Eckert, C. B. Knobler and O. M. Yaghi, *J. Phys. Chem. C.* **2012**, *116*, 13143.

2   S. Keskin and S. Kızılel, *Ind. Eng. Chem. Res.* **2011**, *50*, 1799.

3   P. Horcajada, C. Serre, M. Vallet-Regí, M. Sebban, F. Taulelle and G. Férey, *Angew. Chem. Int. Ed. Engl.* **2006**, *45*, 5974.

4   W. J. Rieter, K. M. Pott, K. M. L. Taylor and W. Lin, *J. Am. Chem. Soc.* **2008**, *130*, 11584.

5   P. Horcajada, C. Serre, G. Maurin, N. A. Ramsahye, F. Balas, M. Vallet-Regí, M. Sebban, F. Taulelle, and G. Férey, *J. Am. Chem. Soc.* **2008**, *130*, 6774.

6   J. An, S. J. Geib and N. L. Rosi, *J. Am. Chem. Soc.* **2009**, *131*, 8376.

7   P. Horcajada, T. Chalati, C. Serre, B. Gillet, C. Sebrie, T. Baati, J. F. Eubank, D. Heurtaux, P. Clayette, C. Kreuz, J.-S. Chang, Y. K. Hwang, V. Marsaud, P.-N. Bories, L.Cynober, S. Gil, G. Ferey, P. Couvreur and R. Gref, *Nat. Mater.* **2010**, *9*, 172.

8   S. R. Miller, D. Heurtaux, T. Baati, P. Horcajada, J.-M. Greneche and C. Serre, *Chem. Commun.* **2010**, *46*, 4526.

9   A. D. Burrows, M. Jurcic, L. L. Keenan, R. A. Lane, M. F. Mahon, M. R. Warren, H. Nowell, M. Paradowski and J. Spencer, *Chem. Commun.* **2013**, *49*, 11260.

10 (a) H. Wu, H. Yu, S. Pan, Z. Huang, Z. Yang, X. Su and K. R. Poeppelmeier, *Angew. Chem. Int. Ed. Engl.* **2013**, *52*, 3406(b) X. Xu, B.-P. Yang, C. Huang and J.-G. Mao, *Inorg. Chem.* **2014**, *53*, 1756(c) G. Zou, L. Huang, N. Ye, C. Lin, W. Cheng and H. Huang, *J. Am. Chem. Soc.* **2013**, *135*, 18560.

11 L. Yang, D. Tao, X. Yang, Y. Li and Y. Guo, *Chem. & Pharm. Bull.* **2003**, *51*, 494.

12 A. S. Prasad, *Mol. Med.* **2008**, *14*, 353.

13 (a) E. Fleige, M. A. Quadir and R. Haag, *Adv. Drug. Deliv. Rev.* **2012**, *64*, 866(b) H. Zheng, C. Gao, B. Peng, M. Shu and S. Che, *J.*

Phys. Chem. C. **2011**, *115*, 7230(c) C. Gao, H. Zheng, L. Xing, M. Shu and S. Che, *Chem. Mater.* **2010**, *22*, 5437(d) Y.-N. Xue, Z.-Z. Huang, J.-T. Zhang, M. Liu, M. Zhang, S.-W. Huang and R.-X. Zhuo, *Polym.* **2009**, *50*, 3706(e) Guo, B.-L. and Gao, Q.-Y. *Carbohydr. Res.* **2007**, *342*, 2416.

14 M. Pourbaix, Atlas of Electrochemical Equilibria in Aqueous Solutions, National Association of Corrosion Engineers, Houston, Tex., 2nd English edn, **1974**.

15 http://www.drugfuture.com/toxic/q71-q610.html.

16 S. K. Kurtz and T. T. Perry, *J. Appl. Phys.* **1968**, *39*, 3798.

17 (a) H.-T. Ye, C.-Y. Ren, G.-F. Hou, Y.-H. Yu, X. Xu, J.-S. Gao, P.-F. Yan and S.-W. Ng, *Cryst. Growth. Des.* **2014**, *14*, 3309(b) Y.-C. He, H.-M.Zhang, Y.-Y. Liu, Q.-Y. Zhai, Q.-T. Shen, S.-Y. Song and J.-F. Ma, *Cryst. Growth. Des.* **2014**, *14*, 3174.

Table of Contents Entry
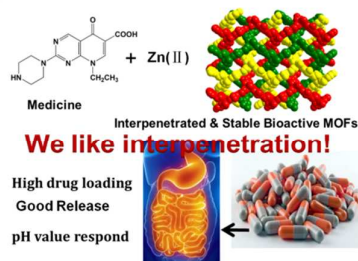
An interpenetrated acentric bioactive MOF with high drug content of 63.9% has been prepared, which shows good release of drug and strong SHG signal.